

# Fabrication of the Fe/PZT Functionally Graded Material and its Application on the Thermal Match for Transducers

Jiangong YU, Zuotong WANG, Bo ZHANG\*, Xiaoming ZHANG, Mo LI

School of Mechanical and Power Engineering, Henan Polytechnic University, Jiaozuo 454003, Henan, China

**crossref** <http://dx.doi.org/10.5755/j02.ms.27727>

Received 25 September 2020; accepted 25 March 2021

To solve the debonding and fracture problems caused by the different thermal expansion coefficients of the transducer element and the measured object, a new method combined with the powder lamination, pressureless infiltration and hot pressing sintering is proposed to prepare Fe/PZT functionally graded material as the matching layer of transducers. The microstructure and element distribution of the functionally graded layer are analyzed by the SEM and EDS. The results show that the volume fraction and elements of the functionally graded layer after the pressureless infiltration at 1100 °C and the hot pressing at 800 °C are linearly and continuously distributed along the thickness direction. The thermal cycle contrast test shows the well matching performance of the functionally graded disk as the transducer matching layer from room temperature to 180 °C. Finally, Lamb wave propagation experiment at the 180 °C shows that the functionally graded matching layer can be used effectively.

**Keywords:** functionally graded material, matching layer, pressureless infiltration, hot pressing sintering, Lamb wave.

## 1. INTRODUCTION

Ultrasonic transducers have been widely used in the non-destructive evaluation. The direct contact high-temperature transducers are very attractive due to their good efficiency and sensitivity [1–4]. In the process of thermal cycle, the thermal expansion coefficients of each element in the sensors do not match. Therefore, it is impossible to realize the long-term on-line condition monitoring. For example, the transducer would be damaged due to the mismatch of thermal expansion coefficients, and the components must be reassembled before each test [5, 6].

The functional graded material (FGM), which has a gradually changed property, is a novel method for solving the interface mutation. It can alleviate or eliminate the debonding failure caused by the different coefficients of thermal expansion of two materials at high temperature [7, 8]. Among numerous methods of manufacturing FGMs, the powder metallurgy has been widely used due to its high reliability and low cost [9, 10]. W/Cu based seven-layered FGM using the spark plasma sintering process was fabricated by Chaubey et al. [11]. The samples sintered at 1050 °C presented excellent mechanical and physical properties. The Al/SiC FGM with 4 layers was fabricated by Surya et al. [12], which was sintered at 580°C in a protected atmosphere furnace. The obtained FGM attained better mechanical properties compared with pure aluminum. The zirconia-based FGM with different thermal expansion coefficients was designed and prepared by Fang et al. [13], which indicated that the stress in the FGM can be adjusted through controlling the distribution of graphite. Fujii et al. [14] developed partially stabilized PSZ-Ti FGMs by the spark plasma sintering (SPS) technique, and they have the ability to prevent the crack propagation in Ti substrates in the fracture toughness tests. A novel approach for

fabrication W/Cu FGM with gradients in hardness and electric conductivity via the microwave processing was proposed by Zhou et al. [15]. The W-Cu FGM with 11 layers by powder stacking was fabricated by Yusefi et al. [16], which has high relative density and excellent sintering behavior. However, among above FGMs fabricated by the powder metallurgy methods, their composition distributions are not continuous. A common strategy is to increase the layer numbers of the powder stack to achieve approximately continuous changes in composition.

There are some other preparation methods to fabricate continuous gradient material, such as centrifugal method or sol-gel method. Watanabe et al. [17] fabricated Al-Al<sub>2</sub>Cu FGM by centrifugal method and investigated the effects of different processing parameters on microstructure distributions. The synthesised SiC-TiC FGM was prepared by Simonenko et al. [18] using the Sol-Gel process. The composition gradient of the SiC-TiC ceramics was confirmed by X-ray computed microtomography. However, the volume fraction distribution can not be easily controlled by these above methods.

In this paper, a novel approach is proposed to fabricate Fe/PZT FGM with linearly continuous variation and easily controlled volume fraction. The technology includes the powder lamination, pressureless infiltration and vacuum hot pressing sintering (vacuum degree is  $6 \times 10^{-6}$ Pa). The principle of this method is to make PVA volatilize and flow out of the pores between the powders at high temperatures, and parts of the interlayer interface are eliminated by the infiltration process of micro melting iron powder. Then, the hot pressing further promotes the flow of internal components, and finally eliminates the interlayer interface to achieve the final effect of continuous change. At last, as the matching layer of transducers, the obtained disk is

\* Corresponding author. Tel.: +86-391-3987501.  
E-mail address: [bozhangpu@163.com](mailto:bozhangpu@163.com) (B. Zhang)

applied into the Lamb wave propagation experiment at high temperatures.

## 2. MATERIALS AND METHODS

The high purity Fe, PVA and PZT powders with average particle size 5  $\mu\text{m}$ , 30  $\mu\text{m}$  and 50  $\mu\text{m}$ , respectively, are used as starting materials for FGM preparation. Four-layered Fe/PZT FGM samples are stacked and compacted according to the design as shown in Fig. 1 with variable wt.% of Fe and PZT (80 % PZT–20 % Fe, 60 % PZT–40 % Fe, 40 % PZT–60 % Fe, 20 % PZT–80 % Fe) in each layer, respectively. Then, 10 wt.% PVA is added into the prepared Fe/PZT powder, and mix them evenly in the planetary ball mill. PVA is as a pore forming agent. The details of ball milling parameters are listed in Table 1.

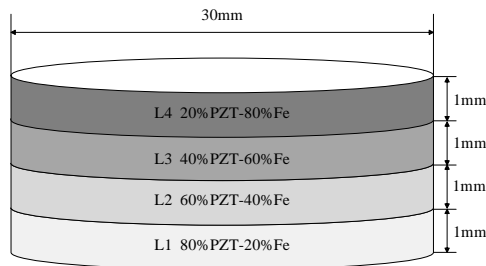


**Fig. 1.** The schematic view of four layers Fe/PZT FGM with varying composition

**Table 1.** Parameters used for milling of the power in planetary ball mill

Property	Fe, PVA and PZT power
Speed	150rpm
Milling time	8h
Grinding medium	Stainless steel balls
Ball to power ratio	10:1
Milling vessel	Stainless steel jar
Milling atmosphere	Normal

The detailed sintering process is as follows. Firstly, the samples are sintered up to 650  $^{\circ}\text{C}$  and kept at this temperature for 30 minutes. Then, the samples are sintered at 1100  $^{\circ}\text{C}$  for 90 minutes. The slightly-melted Fe penetrates into the voids of the lower layer left by the volatilization of PVA. The infiltration of slightly-melted Fe eliminates the interfaces. The values of sintering temperature 1100  $^{\circ}\text{C}$  and the holding time 90 minutes are obtained through a deal of sintering experiments [19, 20]. An excessive temperature (1200  $^{\circ}\text{C}$ , 60 min) or long holding time (1100  $^{\circ}\text{C}$ , 120 min)

would cause an excessive loss of Fe. On the contrary, the permeation is so insufficient that continuous gradient changes can not be formed. Finally, the sintered FGM samples are densified by the vacuum hot pressing at 800  $^{\circ}\text{C}$  and 30 MPa for 90 minutes.

After the final treatment and polishing, the Scanning Electron Microscopy (SEM, Merlin Compact, Zeiss, Germany) equipped with an energy dispersive X-ray spectrometer (EDS) is utilized to evaluate the morphology and element distribution at cross section surfaces.

## 3. PROPERTY ANALYSIS

### 3.1. Fe/PZT FGM microstructure

The backscattered electron image of the hot-pressed sintered sample at 1100  $^{\circ}\text{C}$  is shown in Fig. 2. Due to the difference of components between each layer, the brightness and morphology of the image are also different. Therefore, the interface between layers is clearly visible. The elemental mapping analysis of Fe-PZT FGM is shown in Fig. 3. According to the result of EDS surface scanning in Fig. 3, the main component of the black area (A) in Fig. 2 is PZT, the white bright spot (B) in the black area is mainly Pb, and the gray smooth part (C) are mainly Fe. Due to the material properties of PZT, it is easy to break and form pits during grinding and polishing. With the gradual increase of Fe, the surface of the sample gradually becomes smooth and flat.

The secondary electron surface morphology of the hot-pressed sample after 1100  $^{\circ}\text{C}$  pressureless infiltration is shown in Fig. 4. After infiltration and hot pressing sintering process, it is discovered that the interface between the layers disappeared completely and the surface morphology of the samples changed uniformly. In order to explore the changes of each element after the infiltration, the line scanning observation is performed in the thickness direction of the sample, as shown in Fig. 5. It can be seen that Fe, Zr, Pb, and Ti all tend to change linearly and continuously. This achievement is attributed to the process of pressureless infiltration and hot pressing. At high temperatures, the PVA leaves pores inside the powder sample after volatilization. Then, after the slight melting of Fe powder, it seeps downward under its own gravity, which makes the distribution of various elements change. The subsequent hot press molding further squeezes and fills Fe and PZT into the pores of the PVA after volatilization. The joint actions of pressureless infiltration and hot-pressing sintering make Fe and PZT vary continuously and uniformly, thus eliminating the interface between layers.

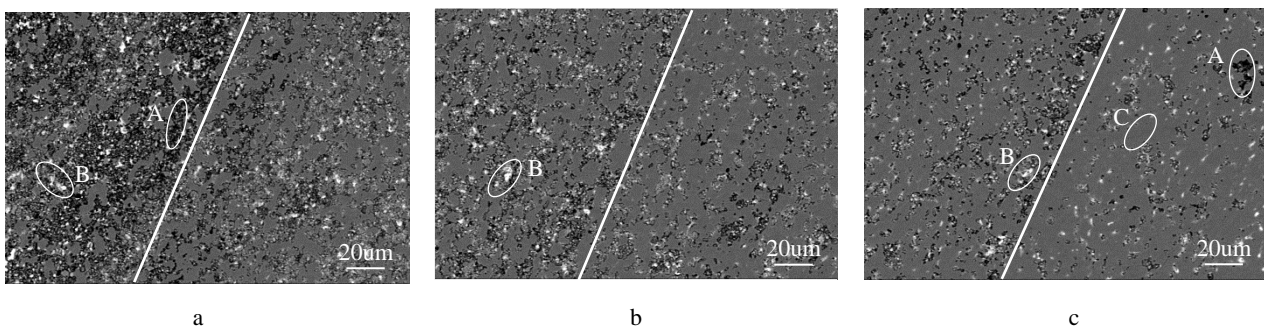


**Fig. 2.** SEM microstructure of the layers (backscattered electron SEM): a – L1-L2 layer; b – L2-L3 layer; c – L3-L4 layer

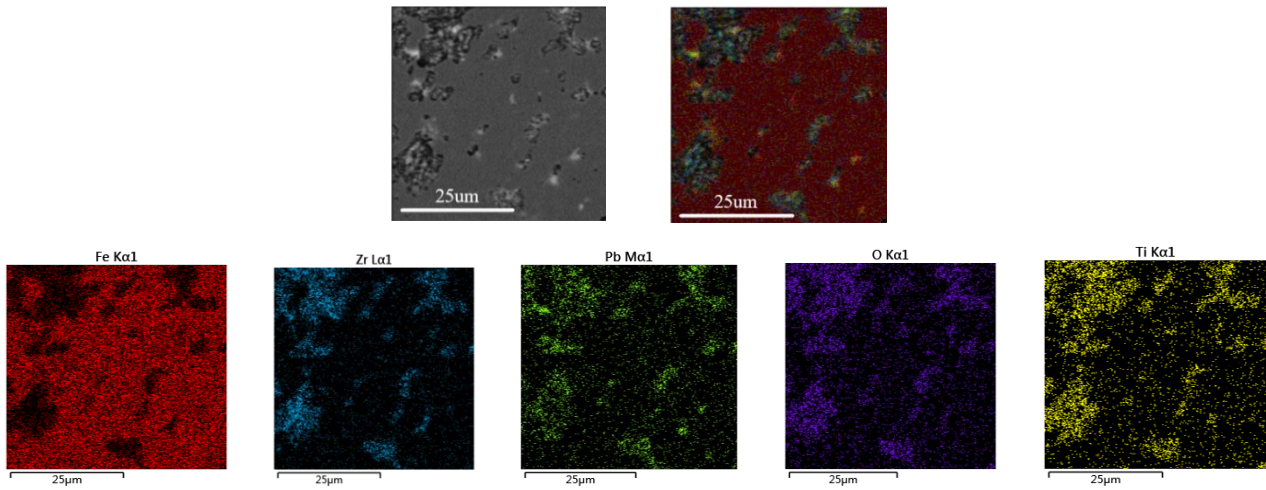


**Fig. 3.** Elemental mapping analysis of Fe-PZT FGM

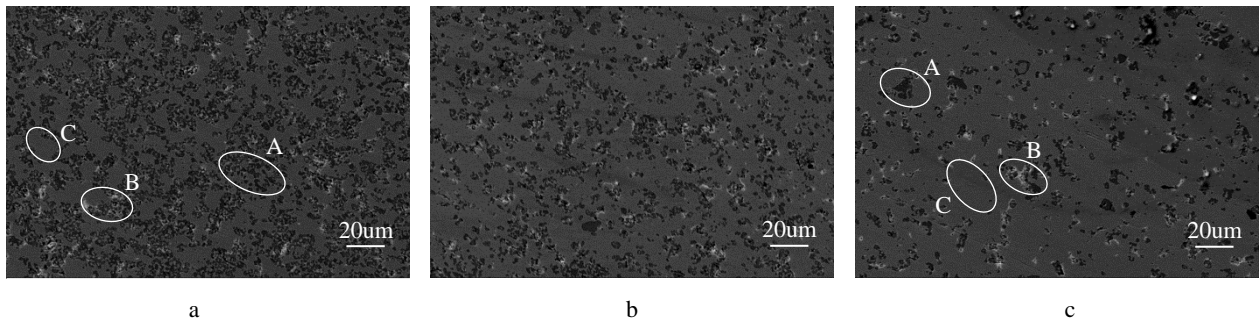


**Fig. 4.** SEM microstructure of the layers (secondary electron SEM): a – L1-L2 layer; b – L2-L3 layer; c – L3-L4 layer

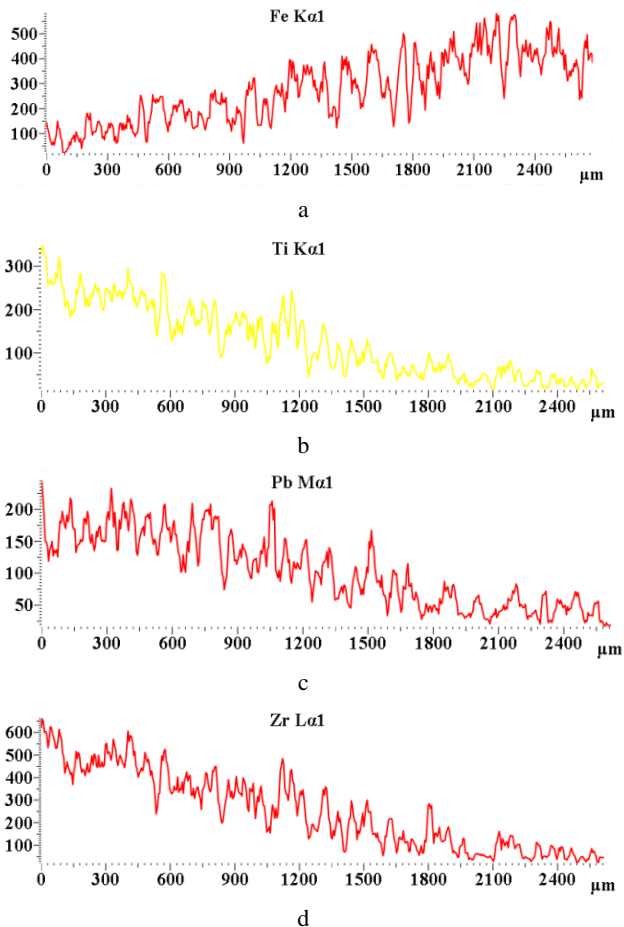


**Fig. 5.** EDS line scan analysis of Fe/PZT

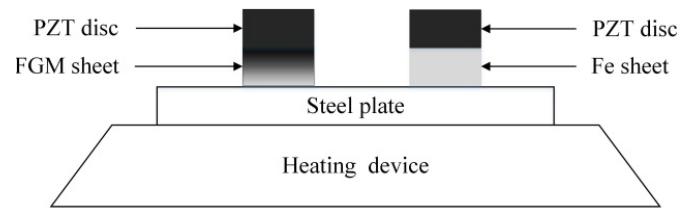


**Fig. 6.** Thermal expansion test device

### 3.2. Thermal expansion matching performance test

In order to test the durability of FGM matching layers when they are repeatedly heated, the FGM and Fe sheet are glued (A-200NL, China) between the PZT disc and Fe sheet, separately. The sketch of the devices is shown in Fig. 6. They are heated repeatedly from room temperature to 180 °C and kept for 30 minutes. The sizes of the PZT disc and Fe sheet are both  $\phi 20 \text{ mm} \times 1 \text{ mm}$ , the steel plate is  $200 \text{ mm} \times 200 \text{ mm} \times 1 \text{ mm}$ . After the hot pressing and sintering process, the FGM thickness is 2.68 mm, which can be seen in the EDS line scan of Fig. 5. To compare with the Fe sheet, the final size of FGM sheet is also  $\phi 20 \text{ mm} \times 1 \text{ mm}$  after grinding and polishing.

It is well-known that stresses would be generated during repeated heating and cooling due to the different thermal expansion coefficients between the Fe sheet and PZT disc. After 61 times hot-cycles, the Fe sheet and PZT disc are separated from each other, as shown in Fig. 7. The FGM sheet and PZT disc are still coupled well even after 200 times hot-cycles, which demonstrates the FGM sheet has a good thermal expansion matching performance from

room temperature to 180 °C. It provides a good idea for solving the mismatch of thermal expansion coefficients between the transducer and the test object at high temperatures.

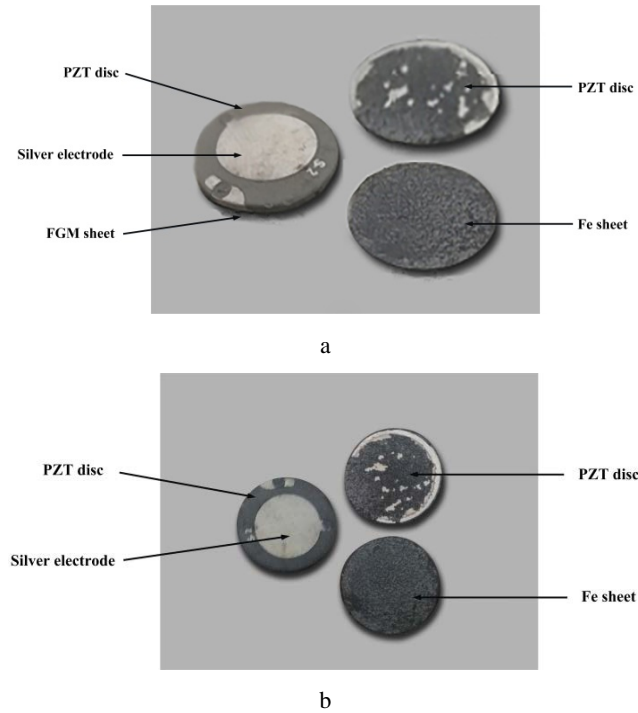


**Fig. 7.** Debonding diagram of PZT disc and Fe sheet at different shooting angles: a–30°; b–90°

#### 4. LAMB WAVE PROPAGATION TEST

Lamb wave is the most common form of guided wave in ultrasonic nondestructive testing. The dispersion curves are important basis for guided wave nondestructive testing, which have been widely investigated [21–23]. To validate the performance of the Fe/PZT FGM matching layer at high temperatures, the Lamb wave propagation experiment is conducted. The experiment devices are illustrated in Fig. 8. In this experiment, the Lamb wave signal with the excitation frequency of 1 MHz is generated by the function generator (RAM-5000-SNAP, RITEC, USA) and loaded on the transducer after being processed by the filter. The transducer generates Lamb wave in the steel plate owing to the piezoelectric effect. In order to reduce the frequency band width of the signal and obtain the waveform with concentrated energy, the excitation signal is a 5-cycle sine wave signal modulated by the Hanning that can be expressed as follows:

$$f(t) = \frac{A}{2} \sin(2\pi f_c t) \left[ 1 - \cos\left(\frac{2\pi f_c t}{5}\right) \right], \quad (1)$$

where  $f_c$  is the center frequency and  $A$  is the signal amplitude.

The acoustic impedance difference between the piezoelectric element and the object to be measured should satisfy the matching requirements. The smaller the acoustic impedance difference, the lower the wave reflectivity at the interfaces. The acoustic impedance of the matching layer can be calculated [24]:

$$Z_m = \sqrt{Z_p \times Z_T}, \quad (2)$$

where  $Z_m$ ,  $Z_p$  and  $Z_T$  are the acoustic impedances of the matching layer, piezoelement and test piece, respectively.

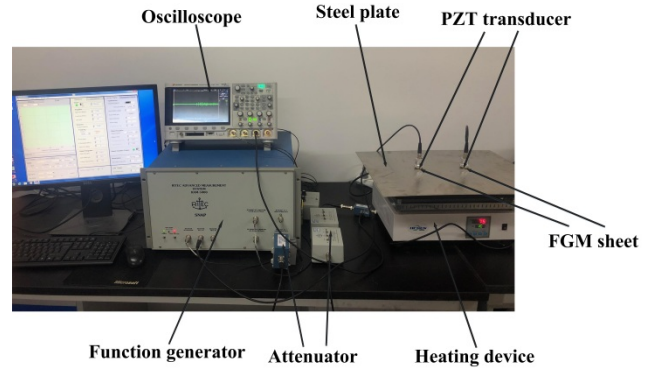


**Fig. 8.** Experimental device for Lamb wave test

The density of 304 stainless steel is  $\rho_1 = 7.9 \times 10^3 \text{ kg/m}^3$ , and the longitudinal wave velocity is  $c_1 = 5640 \text{ m/s}$ . The density of PZT4 is  $\rho_2 = 7.5 \times 10^3 \text{ kg/m}^3$ , and the longitudinal wave velocity is  $c_2 = 4600 \text{ m/s}$ . From  $Z = \rho c$ , the acoustic impedance of 304 stainless steel is  $Z_T = 44.556 \text{ MRals}$ , and that of the PZT4 ceramic is  $Z_p = 34.5 \text{ MRals}$ . Therefore, introducing  $Z_T$  and  $Z_p$  into Eq. 2, the acoustic impedance for the matching layer is  $Z_m = 39.21 \text{ MRals}$ . The acoustic impedance for the matching layer is between those of 304 stainless steel and the PZT4 ceramic. Therefore, the matching layer can be as a transition layer to reduce the acoustic impedance difference. Thus, the wave reflectivity would decrease greatly, the energy transmittance of transducers increases, and the sensitivity and resolution of transducers are improved greatly.

The thickness of the matching layer should be selected as one quarter wavelength at the resonant frequency of piezoelements [24]. The resonant frequency of PZT is 1 MHz. The longitudinal wave velocity  $v$  is 5120 m/s.  $\lambda = v/f = 5.12 \text{ mm}$ , so the thickness of FGM matching layer is 1.28 mm.

In this study, the size of FGM matching layer after grinding and polishing is  $\phi 20 \text{ mm} \times 1.28 \text{ mm}$ , and that of the steel plate is  $1000 \text{ mm} \times 1000 \text{ mm} \times 1 \text{ mm}$ . According to the signal envelope, the propagation time of each wave packet can be obtained, and the propagation speed of the wave packet can be calculated by  $V = s/t$ , where  $s$  is distance between two matching layers, and  $t$  is the propagation time. Since the propagation speed of each wave packet is different, the mode of the wave packet can be determined [25].

Fig. 9 shows the obtained Lamb wave signal at different temperatures. The distance between the two transducers is 500 mm. The interval time corresponding to the maximum value of wave packets at 20 °C and 180 °C is 101.44  $\mu\text{s}$  and 102.96  $\mu\text{s}$ , respectively. The excitation signal duration is 5  $\mu\text{s}$ . Therefore, the propagation time of two wave packets are 98.94  $\mu\text{s}$  and 103.06  $\mu\text{s}$ , respectively. The propagation velocities of the two wave packets are 5054 m/s and 5022 m/s, respectively. According to the dispersion curve [25], it can be determined that this mode is S0 mode, and the theoretical velocity is 5155 m/s, both errors are within

3.5 %. According to the test at 180 °C, the propagating velocity becomes slow because the materials become soft. The test at 180 °C indicates the fabricated FGM sheet can work well as the matching layer.

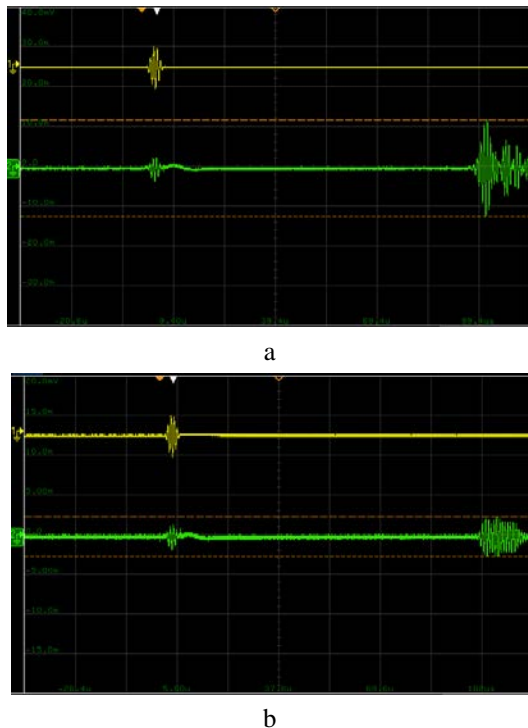


**Fig. 9.** Lamb wave signal in 1mm steel plate: a – 20 °C; b – 180 °C

## 5. CONCLUSIONS

A novel approach combined with the powder lamination, pressureless infiltration and vacuum hot pressing sintering is proposed to fabricate Fe/PZT FGM with linearly continuous variation and easily controlled volume fraction. Then, properties of the prepared Fe/PZT FGM are analyzed using the SEM and EDS. At last, as the matching layer of transducers, the obtained disk is applied into the Lamb wave propagation experiment at 180 °C. Based on above results, the following conclusions can be drawn:

1. The Fe/PZT FGM with linearly continuous variation and easily controlled volume fraction is fabricated by the presented method.
2. SEM photos and EDS line scan confirm the fabricated FGM approaching a continuously changed volume fraction in the thickness direction.
3. When the FGM sheet was used as the transducer matching layer, it can effectively deal with the debonding failure caused by different thermal expansion coefficients between the transducer and the measured object as temperature changes.

## Acknowledgements

The authors gratefully acknowledge the support by the National Natural Science Foundation of China (No. U1804134 and 51975189), and the Training Plan of Young Key Teachers of Universities in Henan Province (No. 2018-GGJS-060).

## REFERENCES

1. **Zhang, S., Yu, F.** Piezoelectric Materials for High Temperature Sensor *Journal of the American Ceramic Society* 94 (10) 2011: pp. 3153–3170. <https://doi.org/10.1111/j.1551-2916.2011.04792.x>
2. **Hashmi, A., Kalashnikov, A.N.** Sensor Data Fusion for Responsive High Resolution Ultrasonic Temperature Measurement Using Piezoelectric Transducers *Ultrasonics* 99 2019: pp. 105969. <https://doi.org/10.1016/j.ultras.2019.105969>
3. **Dhutti, A., Tumin, S.A., Mohimi, A., Kostan, M., Gan, T., Balachandran, W., Selcuk, C.** Development of Low Frequency High Temperature Ultrasonic Transducers for In-service Monitoring of Pipework in Power Plants *Procedia Engineering* 168 2016: pp. 983–986. <https://doi.org/10.1016/j.proeng.2016.11.321>
4. **Fei, C., Zhao, T., Zhang, J., Quan, Y., Wang, D., Yang, X., Chen, Q., Lin, P., Li, D., Yang, Y., Dong, S., Ren, W., Shung, K., Zhou, Q.** 0.36BiScO<sub>3</sub>-0.64PbTiO<sub>3</sub> Piezoelectric Ceramics for High Temperature Ultrasonic Transducer Applications *Journal of Alloys and Compounds* 743 2018: pp. 365–371. <https://doi.org/10.1016/j.jallcom.2018.01.393>
5. **Parks, D.A., Zhang, S., Tittmann, B.R.** High-temperature (> 50 °C) Ultrasonic Transducers: An Experimental Comparison among Three Candidate Piezoelectric Materials *IEEE Transactions on Ultrasonics Ferroelectrics and Frequency Control* 60 (5) 2013: pp. 1010–1015. <https://doi.org/10.1109/TUFFC.2013.2659>
6. **Zhang, X., Li, Z., Wang, X., Yu, J.** The Fractional Kelvin-Voigt Model for Circumferential Guided Waves in a Viscoelastic FGM Hollow Cylinder *Applied Mathematical Modelling* 89 2021: pp. 299–313. <https://doi.org/10.1016/j.apm.2020.06.077>
7. **Udupa, G., Rao, S.S., Gangadharan, K.V.** Functionally Graded Composite Materials: An Overview *Procedia Materials Science* 5 2014: pp. 1291–1299. <https://doi.org/10.1016/j.mspro.2014.07.442>
8. **Parida, S.P., Jena, P.C.** An Overview: Different Manufacturing Techniques used for Fabricating Functionally Graded Material *Materials Today: Proceedings* 2019: pp. 2942–2951. <https://doi.org/10.1016/j.matpr.2019.07.164>
9. **Murr, L.E.** Metallurgy Principles Applied to Powder Bed Fusion 3D Printing/additive Manufacturing of Personalized and Optimized Metal and Alloy Biomedical Implants: An Overview *Journal of Materials Research and Technology* 9 (1) 2020: pp. 1087–1103. <https://doi.org/10.1016/j.jmrt.2019.12.015>
10. **Akhtar, S., Saad, M., Misbah, M.R., Sati, M.C.** Recent Advancements in Powder Metallurgy: A Review *Materials Today: Proceedings* 5 (9) 2018: pp. 18649–18655. <https://doi.org/10.1016/j.matpr.2018.06.210>
11. **Chaubey, A.K., Gupta, R., Kumar, R., Verma, B., Kanpara, S., Bathula, S., Khirwadkar, S.S., Dhar, A.** Fabrication and Characterization of W-Cu Functionally Graded Material by Spark Plasma Sintering Process *Fusion Engineering and Design* 135 2018: pp. 24–30. <https://doi.org/10.1016/j.fusengdes.2018.07.010>
12. **Surya, M.S., Nilesh, T.V.** Synthesis and Mechanical Behaviour of (Al/SiC) Functionally Graded Material Using Powder Metallurgy Technique *Materials Today: Proceedings* 18 2019: pp. 3501–3506. <https://doi.org/10.1016/j.matpr.2019.07.278>

13. **Fang, Y., Su, Y., Zhang, Y., Hu, L.** Design, Preparation and Performance Optimization of Zirconia-based Functionally Graded Materials *Journal of the Chinese Ceramic Society* 44 (12) 2016: pp. 1729–1735.  
<https://doi.org/10.14062/j.issn.0454-5648.2016.12.09>
14. **Fujii, T., Tohgo, K., Isono, H., Shimamura, Y.** Fabrication of a PSZ-Ti Functionally Graded Material by Spark Plasma Sintering and its Fracture Toughness *Materials Science and Engineering A* 682 (13) 2017: pp. 656–663.  
<https://doi.org/10.1016/j.msea.2016.11.091>
15. **Zhou, C., Li, L., Wang, J., Yi, J., Peng, Y.** A Novel Approach for Fabrication of Functionally Graded W/Cu Composites via Microwave Processing *Journal of Alloys and Compounds* 743 2018: pp. 383–387.  
<https://doi.org/10.1016/j.jallcom.2018.01.372>
16. **Yusefi, A., Parvin, N., Mohammadi, H.** W–Cu Functionally Graded Material: Low Temperature Fabrication and Mechanical Characterization *Journal of Physics and Chemistry of Solids* 115 2018: pp. 26–35.  
<https://doi.org/10.1016/j.jpcs.2017.11.029>
17. **Watanabe, Y., Hattori, Y., Sato, H.** Distribution of Microstructure and Cooling Rate in Al–Al<sub>2</sub>Cu Functionally Graded Materials Fabricated by a Centrifugal Method *Journal of Materials Processing Technology* 2015: pp. 197–204.  
<https://doi.org/10.1016/j.jmatprotec.2015.01.028>
18. **Simonenko, E.P., Simonenko, N.P., Nikolaev, V.A., Papynov, E.K., Shichalin, O.O., Gridasova, E.A., Maiorov, V.Y., Grishin, A.V., Sevastyanov, V.G., Kuznetsov, N.T.** Sol–Gel Synthesis of Functionally Graded SiC–TiC Ceramic Material *Russian Journal of Inorganic Chemistry* 64 (11) 2019: pp. 1456–1463.  
<https://doi.org/10.1134/S0036023619110202>
19. **Bochenek, D., Niemiec, P., Szafraniak-Wiza, I., Dercz, G.** Comparison of Electrophysical Properties of PZT-Type Ceramics Obtained by Conventional and Mechanochemical Methods *Materials* 12 (20) 2019: pp. 3301.  
<https://doi.org/10.3390/ma12203301>
20. **Ji, K., Meng, Y., Wang, F., Li, Y.** Influence of Sintering Process on Microstructure and Mechanical Properties of Ti(C,N)-Based Cermet *Materials* 13 (18) 2020: pp. 3938.  
<https://doi.org/10.3390/ma13183938>
21. **Chen, J., Li, Z., Gong, K.** Nondestructive Testing Method Based on Lamb Waves for Localization and Extent of Damage *Acta Mechanica Solida Sinica* 30 (1) 2017: pp. 65–74.  
<https://doi.org/10.1016/j.camss.2016.06.001>
22. **Cho, H., Hasanian, M., Shan, S., Lissenden, C.J.** Nonlinear Guided Wave Technique for Localized Damage Detection in Plates with Surface-Bonded Sensors to Receive Lamb Waves Generated by Shear-Horizontal Wave Mixing *NDT and E International* 102 2019: pp. 35–46.  
<https://doi.org/10.1016/j.ndteint.2018.10.011>
23. **Yu, H., Wang, X.** Dispersion Characteristics of Wave Propagation in Layered Piezoelectric Structures: Exact and Simplified Models *Wave Motion* 96 2020: pp. 102559.  
<https://doi.org/10.1016/j.wavemoti.2020.102559>
24. **Amini, M.H., Sinclair, A.N., Coyle, T.W.** A New High-Temperature Ultrasonic Transducer for Continuous Inspection *IEEE Transactions on Ultrasonics Ferroelectrics and Frequency Control* 63 (3) 2016: pp. 448–455.  
<https://doi.org/10.1109/TUFFC.2016.2519348>
25. **Li, H., Xu, H.** Experimental on the Excitability of Ultrasonic Guided Waves Actuated by Piezoelectric Wafer *Nondestructive Testing* 35 (1) 2013: pp. 22–26. (in Chinese)



© YU et al. 2022 Open Access This article is distributed under the terms of the Creative Commons Attribution 4.0 International License (<http://creativecommons.org/licenses/by/4.0/>), which permits unrestricted use, distribution, and reproduction in any medium, provided you give appropriate credit to the original author(s) and the source, provide a link to the Creative Commons license, and indicate if changes were made.